Electronic Supplementary Information

A low-cost and high-performance 3D micromixer over a wide working range and its application for high-sensitivity biomarker detection

Bo Liu [a b c], Bin Ran [a b c], Chaozhan Chen [a b c], Liuyong Shi [d], Ya Liu [e f], Huaying Chen [b c], Yonggang Zhu [a b c*]

[a.] School of Science, Harbin Institute of Technology, Shenzhen, Shenzhen, 518055, China

[b.] School of Mechanical Engineering and Automation, Harbin Institute of Technology, Shenzhen, Shenzhen, 518055, China

[c.] Center for Microflows and Nanoflows, Harbin Institute of Technology, Shenzhen, Shenzhen, 518055, China

[d.] Mechanical and Electrical Engineering College, Hainan University, Haikou 570228, China

[e.] BGI-Shenzhen, Shenzhen 518083, China

[f.] Shenzhen Key Laboratory of Single-Cell Omics, BGI-Shenzhen, Shenzhen, 518100, China

*Corresponding Author: zhuyonggang@hit.edu.cn

Contents

1. Introduction of equations – Eq. A.1-A.7

The mixing efficiency (ME) of the micromixer at every given position can be calculated according to the following equation[1, 2].

$$ME = 1 - \frac{\sqrt{\sum_{i=1}^{N} (x_i - \overline{x})^2 \Big/ N}}{\overline{x}} \quad \text{(Eq. A.1)}$$

where x_i and $\overline{x}$ is the intensity of each point in the cross-section and the average intensity of all points, respectively. *N* is the total number of points of the cross-section.

Ideally, the value of ME is a maximum of 1, when the solutions achieve complete mixing. Actually, the maximum ME often cannot reach 1[1], infected by the experimental condition and light-admitting quality of material surface, and the solutions (ME≥0.9)[1, 3] are usually regarded as the complete mixing. To accurately understand the mixing performance of the mixer, the relative mixing efficiency [4] (RME) is defined as the following equation (Eq. A.2). In this study, REM (Eq. A.2) was adopted to show the ME of micromixers.

$$RME = \frac{ME}{ME_{complete}} \quad \text{(Eq. A.2)}$$

Where, $ME_{complete}$ is the ME of the completely mixed solution which was pre-mixed well on a magnetic stirrer and flowed into the mixer through the two inlets.

The continuity equation is defined as:

$$\frac{\partial u_k}{\partial x_k} = 0 \quad \text{(Eq. A.3)}$$

Where, u_k is the velocity component in the *k* direction.

The momentum equation is defined as:

$$u_k \frac{\partial u_i}{\partial x_k} = -\frac{1}{\rho}\frac{\partial p}{\partial x_i} + \frac{\mu}{\rho}\frac{\partial}{\partial x_k}\left(\frac{\partial}{\partial x_k} u_i\right) \quad \text{(Eq. A.4)}$$

Where, p, μ and ρ are the pressure, viscosity, and density of the fluid, respectively.

Moreover, concentration fields of 3D micromixers were obtained by solving the convection-diffusion equation for colored species, as shown in the following equation.

$$u_k \frac{\partial c}{\partial x_k} = D\frac{\partial}{\partial x_k}\left(\frac{\partial c}{\partial x_k}\right) \quad \text{(Eq. A.5)}$$

Where c and D are the species concentration and diffusion coefficient, respectively.

To evaluate how rapidly the fluids were mixed, the mixing time taken in the mixing domain was calculated by the following equation[1].

$$t_{\text{mixing}} = \frac{V_{mix}}{Q_{total}} \quad \text{(Eq. A.6)}$$

Where, V_{mix} is the volume of the mixing channel, and Q_{total} is the total flow rate of the two inlets.

2. Experimental setup for measuring mixing performance and pressure drop – Fig. A.1

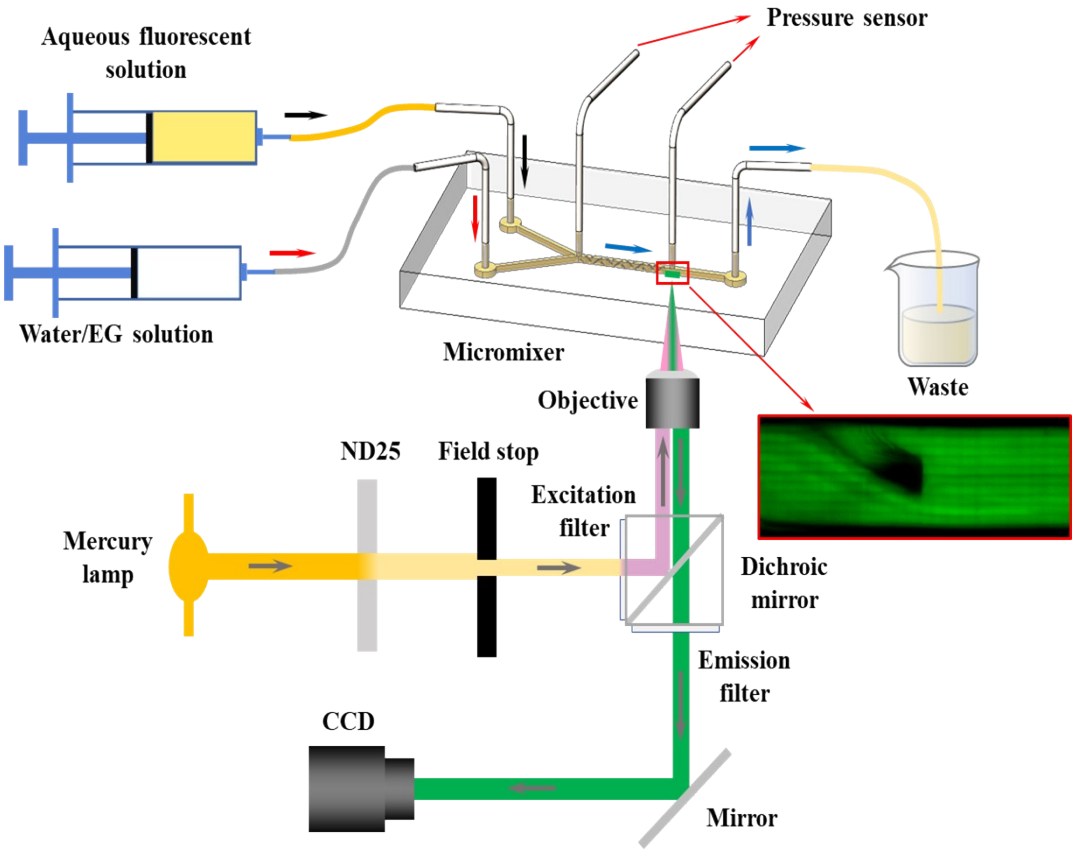

Fig. A.1. Experimental setup for measuring mixing performance and pressure drop. The inlets of micromixer were pumped with aqueous fluorescent solution and water or EG solutions with different concentrations (30%, 50%, 70%, and 90% (v/v)), respectively.

3. Microscopic images of channels and ridges with different design sizes – Fig. A.2

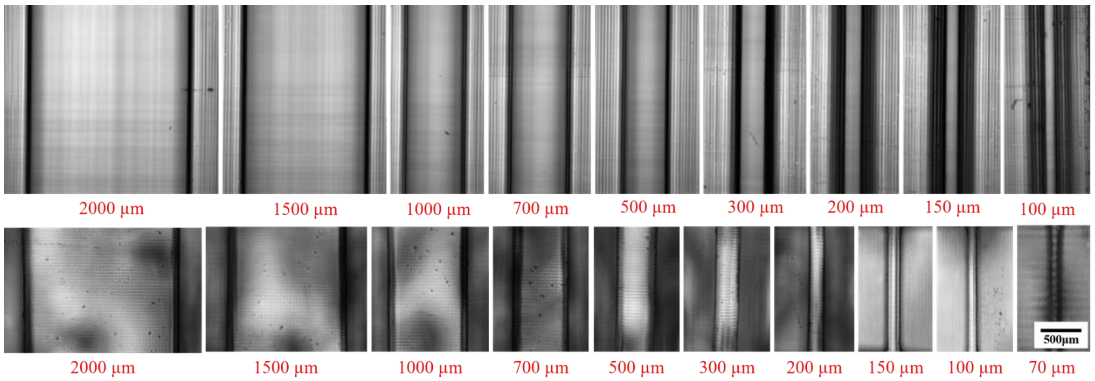

Fig. A.2. Microscopic images of channels and ridges with different design sizes.

4. Three meshes for grid independence study – Table A.1

Table A.1. Three meshes for grid independence study.

Name	First	Second	Third
Max cell size (mm)	0.041	0.032	0.029
Total mesh cells	789,350	1,540,867	2,005,618

5. Streamline and concentration distributions of the cross-section – Fig. A.3

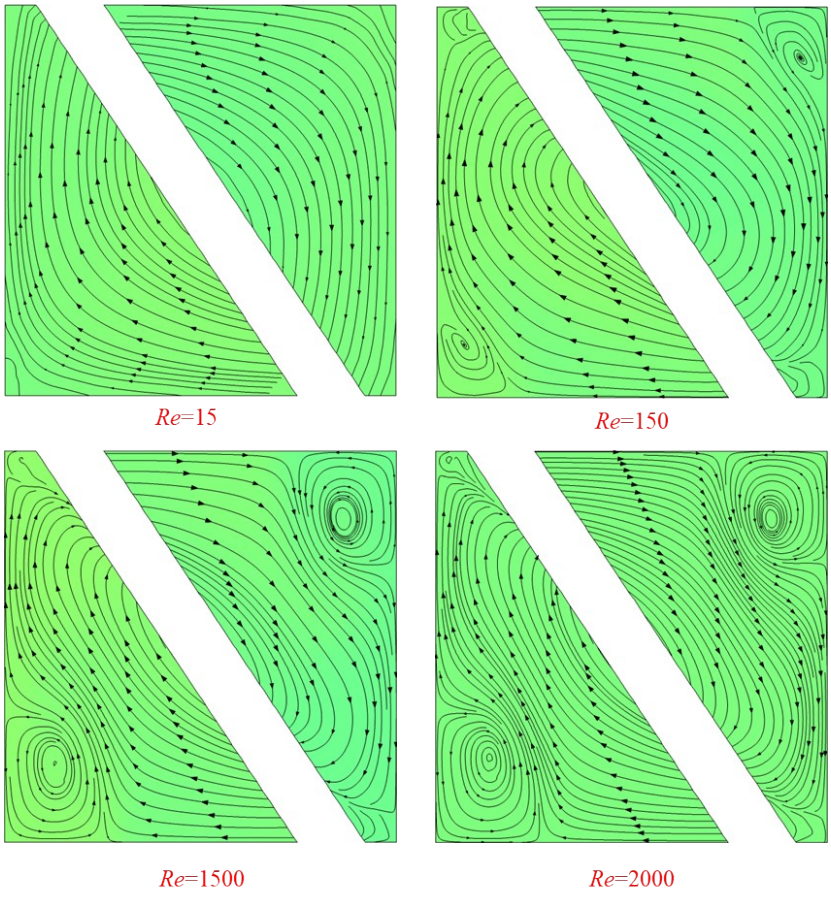

Fig. A.3. Streamline and concentration distributions of the cross-section at different Reynolds numbers.

6. Streamline distribution in the microchannel for µKSM – Fig. A.4

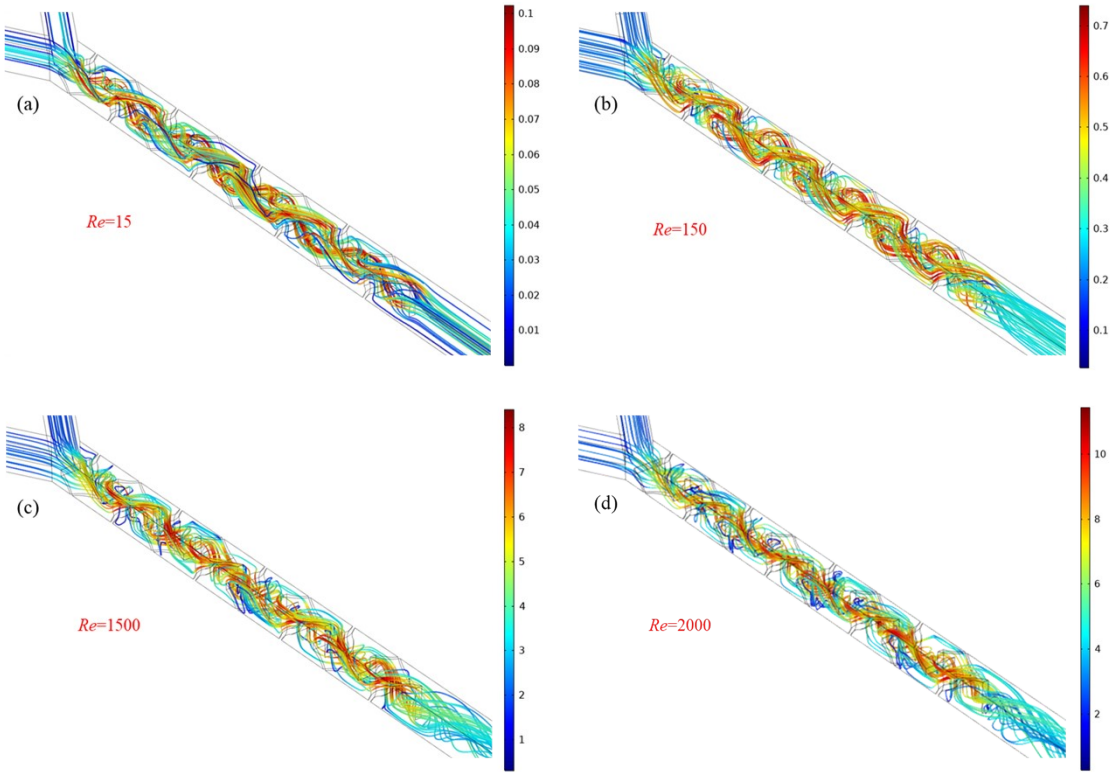

Fig. A.4. Streamline distribution in the microchannel for µKSM at different Reynolds numbers. (a), (b), (c), and (d) streamline distribution at the *Re* of 15, 150, 1500, and 2000, respectively. The color bar means the equivalent velocity in the microchannel, and the bar unit is m s^{-1}.

7. Three structures of helical elements of µKSM – Fig. A.5

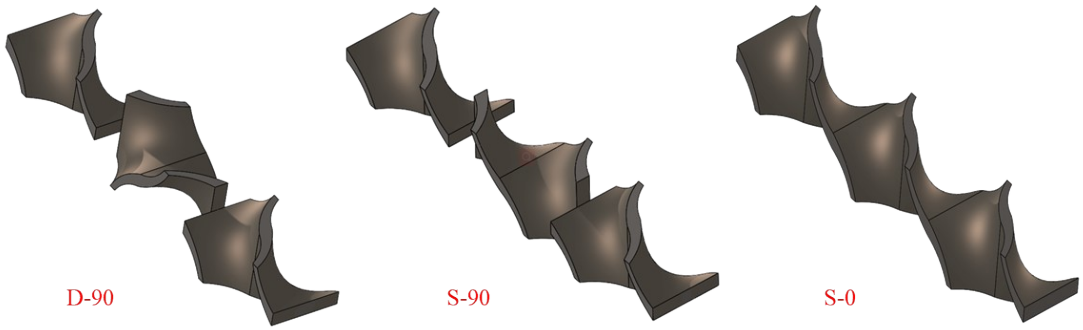

Fig. A.5. Three structures of helical elements of µKSM. D-90, S-90, and S-0 mean elements with different rotation directions and a connection angle of 90°, same rotation direction with a connection angle of 90°, and same rotation direction with a connection angle of 0°, respectively.

8. Streamline distribution in the microchannel for μKSM – Fig. A.6

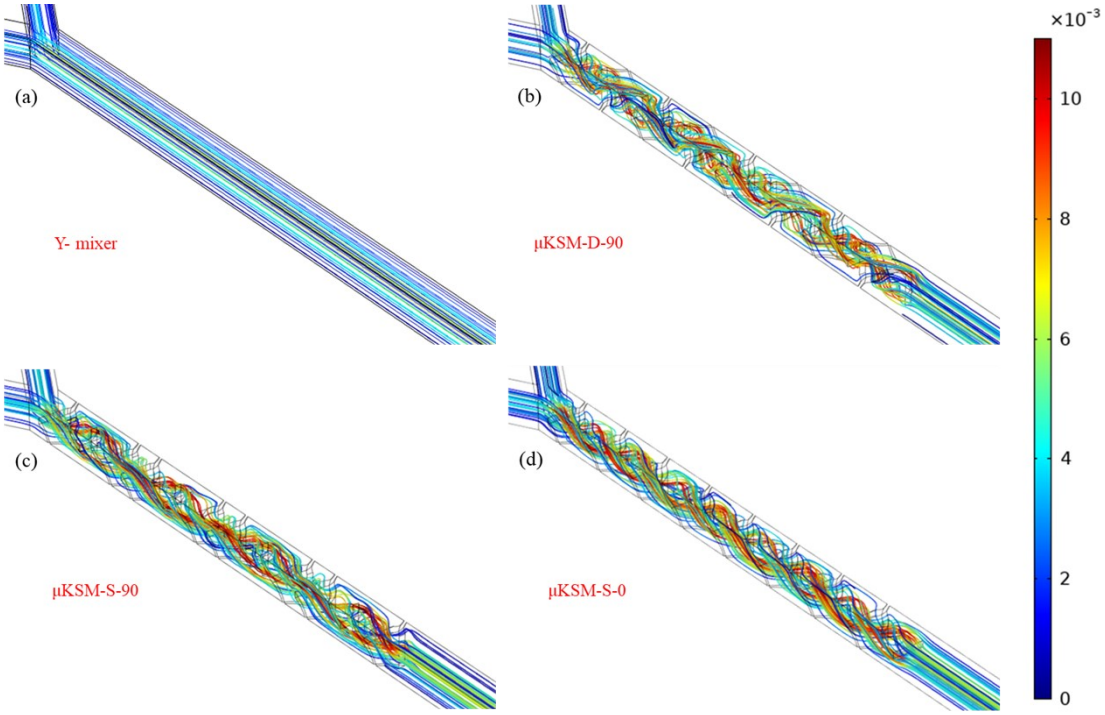

Fig. A.6. Streamline distribution in the microchannel for Y mixer and μKSM with different rotation directions and connect angles at a Re of 1.7. (a) Y mixer without any structure. (b), (c) and (d) μKSM with different rotation directions and a connect angle of 90°, same rotation direction and a connect angle of 90°, and same rotation direction and a connect angle of 0°, respectively. The color bar means the equivalent velocity in the microchannel, and the bar unit is $m \cdot s^{-1}$.

9. Numerical results of concentration distribution with different parameters – Fig. A.7

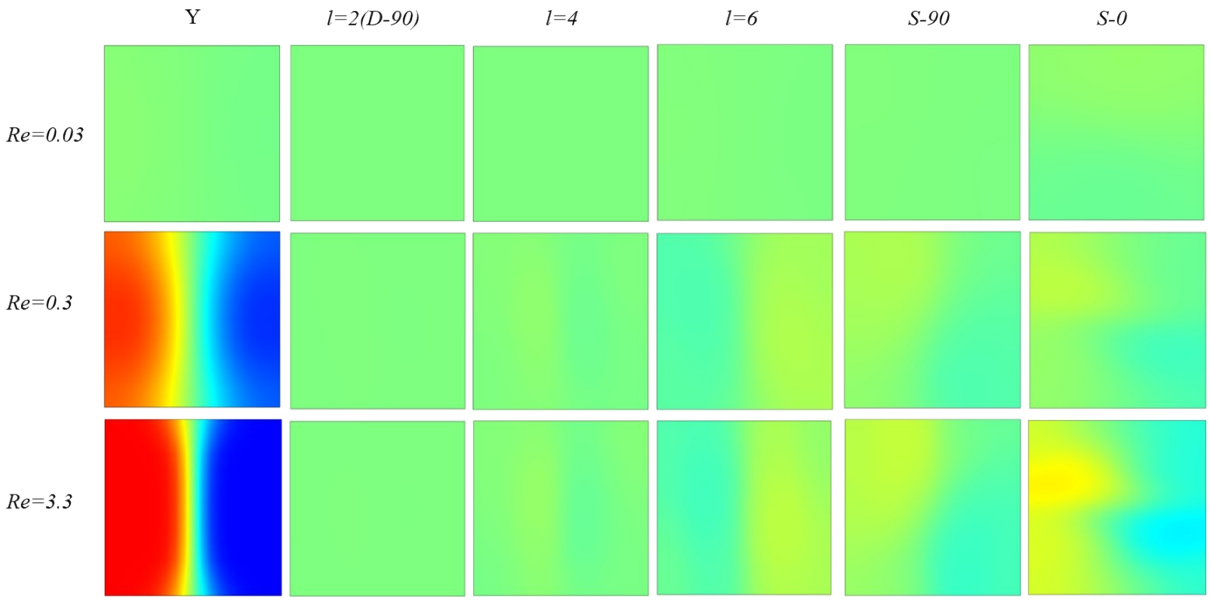

Fig. A.7. Numerical results of concentration distribution (*L*=1) at different *Re* (0.03, 0.3, and 3.3) with different parameters (length, rotation direction, and connect angle of helical element) of μKSM.

10. Fluorescein images of different types of micromixers – Fig. A.8

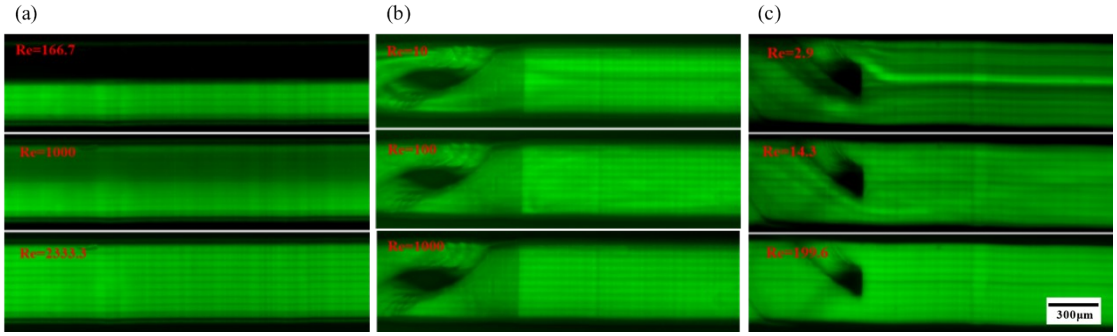

Fig. A.8. Fluorescein images of different types of micromixers at different Reynolds numbers. (a) Microscope fluorescein images of simple Y mixer at mixing length of 1 with Re of 166.7, 1000, and 2333.3. (b) Microscope fluorescein images of μKSM at the mixing length of 0.56 with *Re* of 10, 100, and 1000. (c) Microscope fluorescein images of μKSM for the 90% EG solution with *Re* of 2.9, 14.3, and 199.6, respectively.

11. Dynamic viscosity of solutions at 20° – Table A.2

Table A.2. Dynamic viscosity of solutions at 20° [5]

Solution (v/v)	Viscosity (mPa·s)	Solution (v/v)	Viscosity (mPa·s)
water	1.005	70% glycol	7.53
30% glycol	2.20	90% glycol	12.95
50% glycol	3.94		

12. Comparison of mixing performance for viscosity solutions – Table A.3

Table A.2. Comparison of mixing performance for viscosity solutions between typical passive micromixers

Type	Flow rate (μL min^{-1})	*Re*	*ME* (%)	Ref.
ω-mixer	50-250	~0.44-2.18(80% glycerol)	~24-90(80% glycerol)	[1]
SAR mixer	100-600	~0.7-4.2(98% glycerol)	~90-97 (98% glycerol)	[6]
Dean flow mixer	5-210	0.23-9.86(80% PEG200)	~45-90(80% PEG200)	[7]
SHM mixer	~0.17-750	0.01-10(80% glycerol)	≧90%(80% glycerol)	[8]
μKSM	0.3-70,000	0.00086-200.95(90% EG)	≧85.1(90% EG)	This study

13. Schematic of the assembled detection platform – Fig. A.9

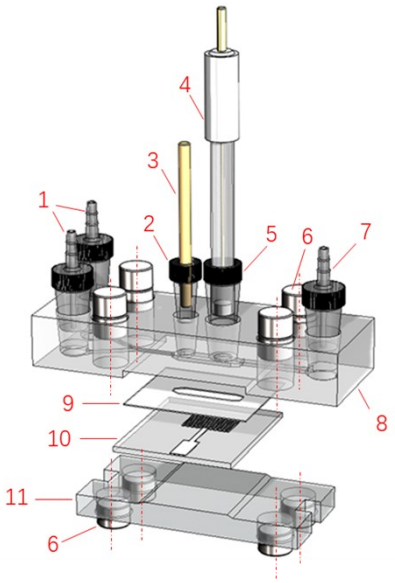

Fig. A.9. Schematic of the assembled detection platform: 1, inlet a and b; 2, a sleeve of CE; 3, CE; 4, RE; 5, a sleeve of RE; 6, magnet; 7, outlet; 8, platform body including microchannel, micromixer and reaction chamber; 9, silicone sheet; 10, WE fabricated by AJP; 11, bottom clamp.

14. Schematic of the designed µEA – Fig. A.10

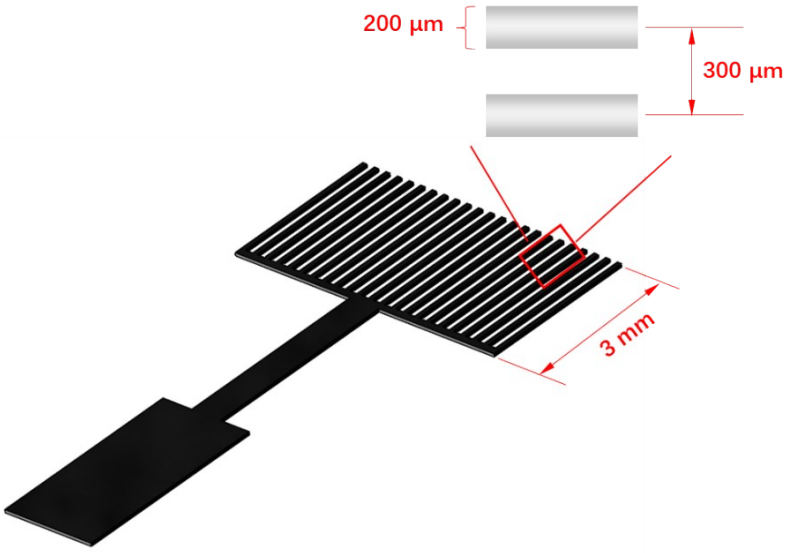

Fig. A.10. Schematic of the designed µEA. The µEA includes 31 silver lines with a space of 300 µm between lines and a width of 200 µm for each line.

15. Schematic of the printing process – Fig. A.11

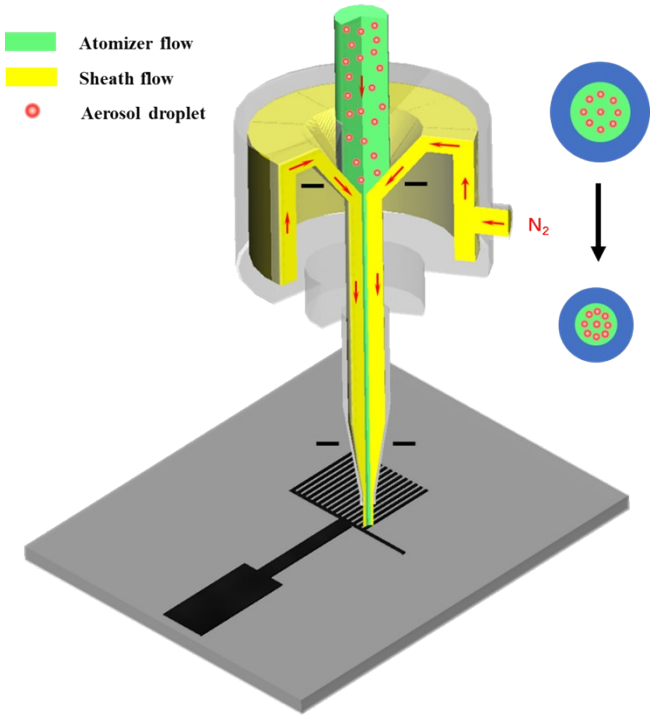

Fig. A.11. Schematic of the printing process. The atomizer flow, including aerosol droplets, was produced by an ultrasonic atomizer. The composition of sheath flow is nitrogen gas. Through the printing head, the atomizer flow is constrained and focused by the sheath flow to form a microjet. The configuration of µEA is printed through the programmed printing head. The µEA is solidified on the heatable printing platform.

16. Experimental results of µEA on the electrochemical detection platform – Fig. A.12

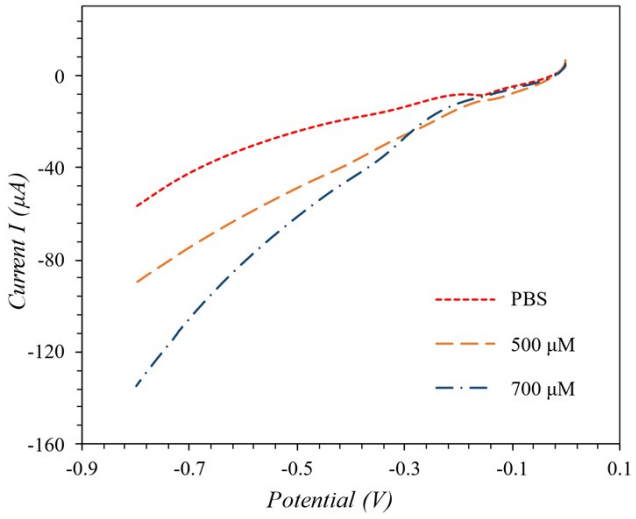

Fig. A12. Linear sweep voltammetry of µEA at a scan rate of 0.05V/s with different concentrations of sarcosine (PBS, 500 and 700µM) at a flow rate of 30µL/min (*Re*≈1).

17. References

1. Y. Li, Y. Xu, X. Feng and B. F. Liu, *Anal Chem*, 2012, **84**, 9025-9032.
2. O. Mihailova, V. Lim, M. J. McCarthy, K. L. McCarthy and S. Bakalis, *Chemical Engineering Science*, 2015, **137**, 1014-1023.
3. J. Y. Wang, C. McMullen, P. Yao, N. D. Jiao, M. Kim, J. W. Kim, L. Q. Liu and S. Tung, *Microfluidics And Nanofluidics*, 2017, **21**.
4. L. Nguyen Hoai An, H. Deng, C. Devendran, N. Akhtar, X. Ma, C. Pouton, H.-K. Chan, A. Neild and T. Alan, *Lab on a Chip*, 2020, **20**, 582-591.
5. S. T. Taylor, *Ashrae Journal*, 1990, **32:2**.
6. H. M. Xia, Z. P. Wang, Y. X. Koh and K. T. May, *Lab Chip*, 2010, **10**, 1712-1716.
7. C. Liu, Y. Li, Y. Li, P. Chen, X. Feng, W. Du and B. F. Liu, *Talanta*, 2016, **149**, 237-243.
8. A. D. Stroock, S. K. Dertinger, A. Ajdari, I. Mezic, H. A. Stone and G. M. Whitesides, *Science*, 2002, **295**, 647-651.